Asymmetric use of 8-legged Conventional Birdcage

Thomas Clerbois*, Antoine Rampelbergh*, Farzad Jabbarigargari*, Chan-Sun Park*, Redha Abdeddaim†, Christophe Craeye*

*Universite catholique de Louvain: ICTEAM, Louvain-la-Neuve, Belgium, tclerbois@gmail.com

†Aix Marseille Univ., CNRS, Centrale Marseille, Institut Fresnel, Marseille, France

***Abstract*—In high-frequency magnetic resonance imaging (MRI) system, shaping of the magnetic field inside the body becomes an important challenge. The choice of the Radio-frequency (RF) coils and their design is essential if a quality image is expected. This paper presents the asymmetric use of a conventional Birdcage RF coil and answers the problem of homogeneity as well as localizing an off-centered region of interest (ROI).**

***Index Terms*—magnetic resonance imaging, radio-frequency coil, birdcage coil, asymmetric birdcage coil.**

I. Introduction

Radio-frequency (RF) coils are essential for each magnetic resonance imaging (MRI) system, since they are responsible for transmitting and receiving the RF pulses. Due to the highly varying field penetration in the different parts of the body, surface or volume coils need to be used [1]. The birdcage coil is the most famous volume coil since it can produce a homogeneous field distribution inside its volume [2]. However, the homogeneity of the fields inside the birdcage coil degenerates at high and ultra-high field (UHF) MRI because of the shortened wavelength inside the body, resulting in bright and dark spots in the field distributions [3]. Several methods like parallel transmission [4], dielectric pads [5], and the HMA method [6], have been used to improve the homogeneity in UHF MRI in the region of interest (ROI). In this paper, an in-house method-of-moments (MoM) code has been used to design and optimize both symmetric and asymmetric birdcage coils to improve the homogeneity of the B_1^+ field (the component of the magnetic field which is used in the transmission mode) in the presence of a dielectric sphere.

II. Methodology

First of all, a high-pass (HP) 8-legged 7T birdcage was used, as represented in Fig. 1. This birdcage has a height of 28 cm, and its radius is 13 cm. As there are 8 legs, this birdcage design contains 16 capacitors. The positions correspond to the HP configurations i.e. on both the top and bottom end-ring sectors. Two excitation ports in the middle of two legs have been used to excite the birdcage coil in quadrature mode. All simulations are realized in the presence of a spherical phantom with a radius of 8 cm, the relative permittivity and conductivity are 45.3 and 0.87 S/m, respectively.

The morphology of the birdcage is designed and adapted using the open-source GMSH meshing software [7].

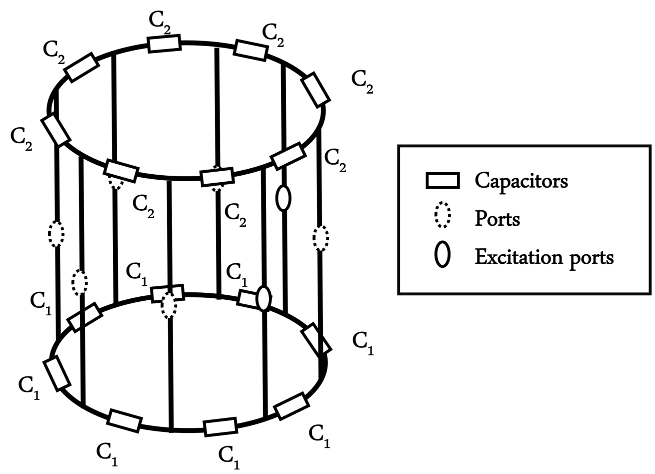

Fig. 1. Capacitor positions for a high pass symmetric Birdcage.

An in-house MoM code is used to compute once the open circuit embedded element pattern [8] and the particle swarm optimization method [9], is used to obtain the optimized capacitor values corresponding to the different cost functions that can be defined to improve the homogeneity on the entire domain or locally.

In order to compare the different results and to analyze the performance of the different designs, a standard metric defined as normalized standard deviation (NSD= $\frac{SD(B_1^+)}{Avg(B_1^+)}$) of the $|B_1^+|$ field, provided in equation (1), is used to compare the results for the transverse plane in the middle of the coils.

$$NSD(B_1^+) = \frac{Std(B_1^+)}{Mean(B_1^+)} \tag{1}$$

where

$$Std(B_1^+) = \sqrt{\frac{\iint |B_1^+(r) - Mean(B_1^+)|^2 ds}{S}} \tag{2}$$

$$Mean(B_1^+) = \frac{\iint |B_1^+(r)| ds}{S} \tag{3}$$

Where S is the area of the ROI.

III. Symmetric case

The symmetric case is named so as both the birdcage, its capacitor values and the used weight matrices are symmetric.

TABLE I
BASIC SYMMETRIC CASE

NSD	C_1 [F]	C_2 [F]
0.2298	8.32e-13	8.32e-13

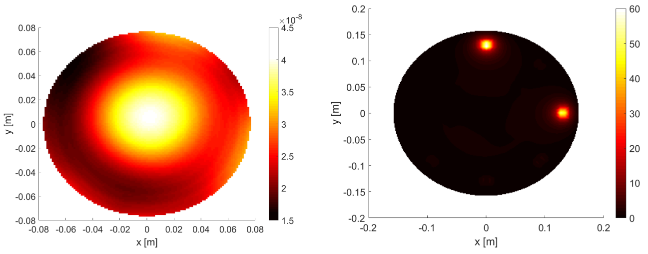

(a) (b)

Fig. 2. (a) SAR efficiency and (b) electric field distribution of the symmetric birdcage.

Therefore, the Birdcage shown in Fig. 1 has only 2 capacitor values, C_1 and C_2, repeated in each leg. The symmetry allows faster and lighter computation and is a useful milestone before switching to the non-symmetrical birdcage.

A. Basic symmetric case

In this case, all capacitors have the same value, but one sits below and one above the horizontal symmetric plane. The metric is used to optimize the magnetic field homogeneity in the transverse cut of the spherical phantom while keeping the birdcage symmetrical.

1) Results and analysis: The resulting specific absorption rate (SAR) efficiency ($\frac{(B_1^+)}{\sqrt{SAR_{max}}}$) and electric field distributions on the transverse cut of the sphere are represented in Fig. 2 while its capacitor values and NSD are presented in Table I.

As shown in Fig. 2a the SAR efficiency is centered and not homogeneous on the sides. Indeed, two small regions have values of around $3 \cdot 10^{-8} \left[\frac{T}{\sqrt{W/Kg}}\right]$ while the rest of the sides has values around $2 \cdot 10^{-8} \left[\frac{T}{\sqrt{W/Kg}}\right]$. The main cause of this inhomogeneity on the sides are the (active) excitation ports. While they are used to excite the desired mode in the birdcage, they create non-negligible hotspots (in yellow) in the E-field on the right and at the top in Fig. 2b. Those translate into decreased SAR efficiency and high NSD.

This basic case is used as a reference when analyzing results obtained in this paper. Both the visual and numerical aspects help understand the improvements brought by the approach.

2) S-parameters analysis: The scattering parameters are shown in Fig. 3, which confirms the proper behaviour of the coil at 7T, by a local minimum both for S_{11} and S_{12}. However, the coil can be tuned an matched to the desired 7T Larmor frequency.

IV. ASYMMETRIC CASE

The birdcage coil presented in the previous section is symmetrical since each sector is identical; however, as shown in Fig. 4, the birdcage can be asymmetric by choosing different values for each capacitor (C_1-C_{16}). The asymmetric case will dive deeper into the possibilities it offers, one of them being the ability to counteract the effect of the excitation ports mentioned in the symmetric case, resulting in an improved homogeneity in the ROI.

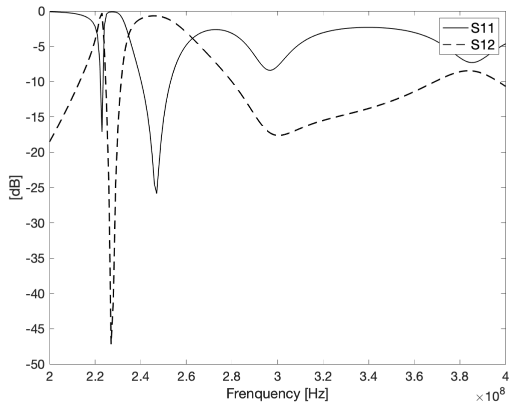

Fig. 3. S-Parameters for the symmetric birdcage.

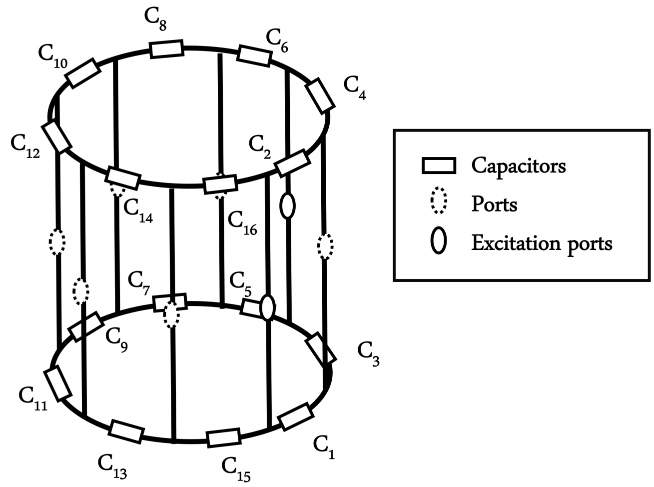

Fig. 4. Capacitors of the asymmetric birdcage.

A. Basic asymmetric case

The resulting SAR efficiency and electric field distributions are represented in Fig. 5, while its C-values are presented in Table II. The main problem mentioned in the symmetric case was the presence of excitation ports with the birdcage not being able to counteract their impact. With the asymmetric configuration of the birdcage however, different C-values are feasible and can be considered as an option to counter this effect. A joint analysis of the numerical values of Table II and Fig. 5b shows a correlation between the capacitors values and the value of the E-field. First, let us clarify that C_1, C_2, C_5 and C_6 are the capacitors on the end ring that are close to the excitation ports and have lower values.

TABLE II
CAPACITOR VALUES FOR THE ASYMMETRIC CASE

C_1 [F]	C_2 [F]	C_3 [F]	C_4 [F]	C_5 [F]	C_6 [F]
8.69e-14	9.54e-14	6.30e-12	5.92e-13	1.43e-13	8.34e-14
C_7 [F]	C_8 [F]	C_9 [F]	C_{10} [F]	C_{11} [F]	C_{12} [F]
1.70e-12	1.17e-12	1.05e-11	2.08e-12	8.35e-13	1.56e-11
C_{13} [F]	C_{14} [F]	C_{15} [F]	C_{16} [F]		
5.24e-12	7.05e-13	1.52e-12	1.84e-12		

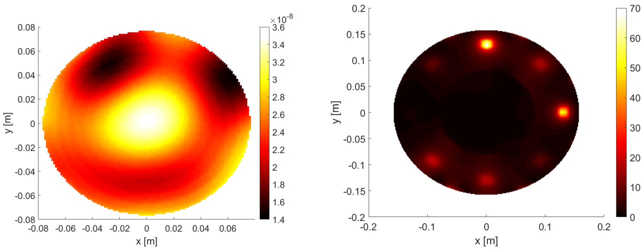

(a) (b)

Fig. 5. (a) SAR efficiency and (b) electric field distribution of the asymmetric birdcage.

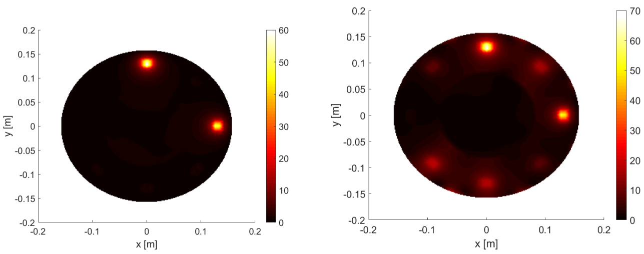

(a) (b)

Fig. 6. Electric field distribution for (a) symmetric birdcage (b) asymmetric birdcage.

All the other capacitors are located on end rings have higher values. It can be said that those higher values compensate the already existing hotspots in the E-field, while the lower values increase the least possible the existing hot spots while respecting the resonance conditions of the Birdcage.

While C_3, C_4, C_7, C_8, C_{15} and C_{16} improve the homogeneity near the excitation ports, the other capacitors take care of the rest of the torus-shaped region defined by the weight matrix. The difference between the resulting E-field for the symmetric and asymmetric cases is shown in Fig. 6. The average capacitors value for the asymmetric case is 4.01e-12 $[F]$ (without C_1, C_2, C_5 and C_6) while the symmetric case has 8.32e-13 $[F]$ capacitors. This is a factor 4.83 of difference, explaining the difference in E-values and visibility of the spots on the graph.

1) Improved homogeneity: As Table III shows, the NSD on the ROI is decreased in the asymmetric configuration by 24%, resulting in the improved homogeneity of the B_1^+ field for the asymmetric coil.

TABLE III
NSD FOR THE SYMMETRIC AND THE ASYMMETRIC BIRDCAGE ON THE TRANSVERSE PLANE INSIDE THE SPHERE

	Symmetric case	Asymmetric case
ROI	0.2298	0.1745

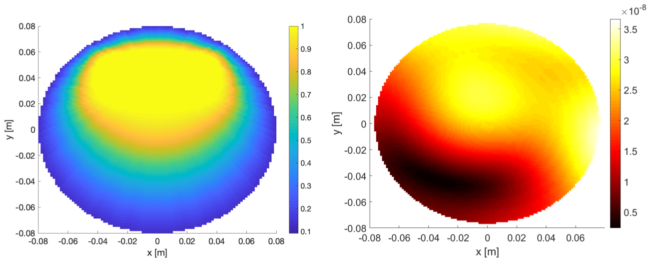

(a) (b)

Fig. 7. (a) Desired weighting matrix (b) obtained field distribution with the asymmetric birdcage.

V. ASYMMETRIC BIRDCAGE FOR SHAPING THE FIELD DISTRIBUTIONS

Instead of analysing the field's homogeneity, a desired shape of the fields is targeted with the asymmetric birdcage in this section.

A. *Weight matrix*

This shape is defined using a weighting matrix, in this case ellipse-shaped, shown in Fig. 7a. Inside the ellipse, the weights are set to 1. Outside the ROI, the weights are defined by a Gaussian based on the distance between the edge of the ROI and the edge of the circle. The ellipse-shaped weight matrix actually combines homogeneity and shape of the field as the ellipse region is homogeneous compared to the rest of the desired field.

B. *Results*

The optimized values of the capacitors are obtained using the MoM code with this weighting matrix. The SAR efficiency corresponding to the weighting matrix described above is shown in Fig. 7b. Indeed, the ellipse-shaped region is clearly located in the top part of the phantom. There is a non-negligible influence of the excitation ports, but it doesn't cause too much damage as the ROI is located close by. Besides the shape of the field distribution, its value are sufficient.

VI. CONCLUSION

This paper proposes an asymmetric design for an eight-legged conventional birdcage coil to improve the homogeneity of the B_1^+ field on the transverse cut inside the spherical phantom. Different values for the capacitors used in each birdcage segment are obtained through the MoM computation, providing the possibility of shaping the field distribution. A significantly improved control over the field distribution is achieved. Real-time control might be obtained using variable capacitors.

References

[1] J.T. Vaughan and J.R. Griffiths,“RF coils for MRI,” John Wiley Sons, 2012.

[2] C.E. Hayes, W.A. Edelstein, J.F. Schenck, O.M. Mueller, and M. Eash, “An efficient, highly homogeneous radiofrequency coil for whole-body NMR imaging at 1.5 T,” Journal of Magnetic Resonance, vol. 63, pp. 622-628, 1985.

[3] C.M. Collins, W. Liu, , W. Schreiber, Q.X. Yang, and M.B. Smith, “Central brightening due to constructive interference with, without, and despite dielectric resonance. Journal of Magnetic Resonance Imaging,” An Official Journal of the International Society for Magnetic Resonance in Medicine, vol. 21, pp. 192-196, 2005.

[4] P. Ullmann, S. Junge, M. Wick, F. Seifert, W. Ruhm, and J. Hennig, “Experimental analysis of parallel excitation using dedicated coil setups and simultaneous RF transmission on multiple channels,” Magnetic Resonance in Medicine: An Official Journal of the International Society for Magnetic Resonance in Medicine, vol. 54, pp. 994-1001, 2005.

[5] A.G. Webb, “Dielectric materials in magnetic resonance,” Concepts in magnetic resonance part A, vol. 38, pp.148-184., 2011.

[6] M. Dubois, L. Leroi, Z. Raolison, R. Abdeddaim, T. Antonakakis, J. De Rosny, A. Vignaud, P. Sabouroux, E.Georget, B. Larrat, and G. Tayeb, “Kerker effect in ultrahigh-field magnetic resonance imaging,” Physical Review X, vol. 8, p. 031083, 2018.

[7] C. Geuzaine and J.F. Remacle, “Gmsh: A 3-D finite element mesh generator with built-in pre-and post-processing facilities,” International journal for numerical methods in engineering, vol. 79, pp. 1309-1331, 2009.

[8] C. Craeye and D. González-Ovejero, “A review on array mutual coupling analysis,”. Radio Science, vol. 46, pp. 1-25, 2011.

[9] J. Kennedy and R. Eberhart, “Particle swarm optimization,” In Proceedings of ICNN’95-international conference on neural networks , vol. 4, pp. 1942-1948, 1995.